Convective heat and mass transfer in wavy finned-tube exchangers

G. Comini, C. Nonino and S. Savino
Università degli Studi di Udine, Dipartimento di Energetica e Macchine, Udine, Italy

Keywords *Numerical simulation, Convection, Heat transfer*

Abstract *The paper adopts a simplified two-dimensional approach to deal with convective heat and mass transfer in laminar flows of humid air through wavy finned-tube exchangers. The computational domain is spatially periodic, with fully developed conditions prevailing at a certain distance from the inlet section. Both the entrance and the fully developed flow region are investigated. In the fully developed region, periodicities in the flow, temperature and mass concentration fields are taken into account. The approach is completely general, even if the finite element method is used for the discretizations. In the application section, velocity, temperature, and mass concentration fields are computed first. Then apparent friction factors, Nusselt numbers, Colburn factors for heat and mass transfer, and goodness factors are evaluated both in the entrance and in the fully developed region.*

Nomenclature

a = thermal diffusivity of humid air
A = peak-to-peak amplitude
d = binary diffusion coefficient for the water vapour – air mixture
D_H = hydraulic diameter
f = friction factor
$\mathbf{g}$ = effective load vector
h = convection heat transfer coefficient
h_m = convection mass transfer coefficient
H = height
$\mathbf{H}$ = effective stiffness matrix
j = Colburn factor for heat transfer
j_m = Colburn factor for mass transfer
L = projected length
m = number of half modules
$\dot{m}$ = mass flow rate
Nu = Nusselt number
p = pressure
$\tilde{p}$ = periodic component of pressure
Pr = Prandtl number
q = heat flow rate
R = gas constant
Re = Reynolds number
S = projected surface
Sc = Schmidt number
Sh = Sherwood number
St = Strouhal number
t = temperature
T = absolute temperature
u, v = velocity components in the (x, y) directions
x, y = Cartesian coordinates
y' = distance from the lower boundary in the y direction

Greek

α = overall pressure gradient in the flow direction
ϕ = dependent variable
$\boldsymbol{\phi}$ = vector of nodal values of ϕ
ν = kinematic viscosity of humid air
ϑ = time
Θ = period
ρ = density of humid air
ω = mass fraction of water vapour

International Journal of Numerical Methods for Heat & Fluid Flow, Vol. 12 No. 6, 2002, pp. 735-755.

DOI 10.1108/09615530210438373

Ω = dimensionless concentration of water vapour
ψ = streamfunction

Subscripts
b = bulk
i = inflow
ml = logarithmic mean
o = outflow
tf = throughflow
v = water vapour
w = wall
∞ = in the fully developed region

Superscripts
n = at the n-th time step
- = space-averaged value

Introduction

Simultaneous heat and mass convection occurs in many cooling systems utilized for summer air-conditioning operations. Typical examples are fan-coil units and evaporators when external surfaces are maintained at temperatures below the dew point. In these apparatuses, the air-side heat transfer coefficient is much smaller than the internal heat transfer coefficient for the refrigerating fluid. To reduce the air-side thermal resistance, recourse is usually made to extended surfaces in the form of fins that increase the external area. In modern exchangers, however, the use of heat transfer enhancement techniques is also required since, to limit the emission of noise, frontal velocities of the humid air are maintained low and the resulting flows, almost invariably, laminar. To increase convection coefficients, specially configurated fins are usually adopted. For example, wavy fins have been employed extensively in the past for their simplicity, and are still preferred today in many low-cost applications.

Two wavy channels of finite width have been investigated by Ali and Ramadhyani (1992). These authors report a flow-visualization study, several data concerning overall friction factors and heat transfer coefficients, and an extensive literature review. Unfortunately, most available datas refer to relatively high Reynolds number flows, overall friction, and heat transfer coefficients. In fact, according to Webb (1994,, p. 110), not much information seem to be available on entrance length effects even though these effects play an important role in continuous fin surfaces. Furthermore, the present authors are not aware of any study that deals with simultaneous heat and mass convection within wavy fin channels.

The aim of this paper is to fill the gaps left by previous investigations, using the finite element approach illustrated by Nonino and Comini (1997, 1998). The proposed methodology is applied first to the computation of velocity, temperature, and mass concentration fields during simultaneous heat and mass convection in the entrance and in the fully developed regions within wavy fin surfaces. Then, the corresponding momentum, heat and mass transfer characteristics are evaluated in terms of friction factors, Nusselt numbers, and Colburn factors for heat and mass convection. Furthermore, the performance of wavy channels relative to plain channels is investigated. The main purpose, however, is to clarify the physics of the process rather than to produce an exhaustive database of numerical results. Thus, the examples of application

concern laminar flows of humid air in the range of Reynolds numbers from 100 to 1,000, but deal with a single representative geometry. For the sake of simplicity, the formulation is developed for two-dimensional domains and disregards the influence of water vapour condensation on the velocity field. Extensions to three-dimensional flows are possible and do not present additional difficulties as demonstrated, for example, by Nonino *et al.* (1999) and Nonino and Comini (2000). On the contrary, the effects of condensation on heat and mass convection coefficients cannot be easily taken into account. However, these effects are not even fully established experimentally, as yet, although it appears that friction factors are always enhanced by the presence of condensation, e.g. see Xu *et al.* (1994) and Ramadhyani (1998).

Statement of the problem

As already pointed out, we are dealing with heat and mass convection in two-dimensional laminar flows of a constant property fluid. By simplifying the flow in an actual tube-fin exchanger to a channel flow between parallel fins, we neglect the effects due to the presence of tubes. However, we can still adequately account for those of the wavy fin geometry, thus allowing significant comparisons with the corresponding plain fins.

According to the two-dimensional approach followed, a typical tube-fin exchanger, such as the one shown in Figure 1(a), is modelled as shown in Figure 1(b). This schematic representation of the entrance region consists of a series of identical geometrical modules. After a short distance from the entrance the velocity, and the dimensionless temperature and mass concentration fields repeat themselves, from module to module, attaining a fully developed character. In the fully developed region, the repetitive fields allow the limitation of the analysis to a single module, such as the one enclosed by the periodic boundaries S_1 and S_3 in Figure 1(c). In the present case, however, it is possible to reduce the computational domain still further. With reference to Figure 1(c), in fact, one can consider only a single half-module, such as the one enclosed by the anti-periodic boundaries S_1 and S_2. On these anti-periodic boundaries, normal velocity components have the same value and the same sign, while tangential velocity components have the same absolute value but opposite sign. The relationships between temperature and mass concentration distributions on S_1 and S_2 can be found, following the procedure shown by Nonino and Comini (1998).

The flow field

Under the assumptions made, the momentum and continuity equations governing the laminar flow of humid air can be written as:

$$\frac{\partial u}{\partial \vartheta} + u\frac{\partial u}{\partial x} + v\frac{\partial u}{\partial y} = \nu\left(\frac{\partial^2 u}{\partial x^2} + \frac{\partial^2 u}{\partial y^2}\right) - \frac{1}{\rho}\frac{\partial p}{\partial x} \tag{1}$$

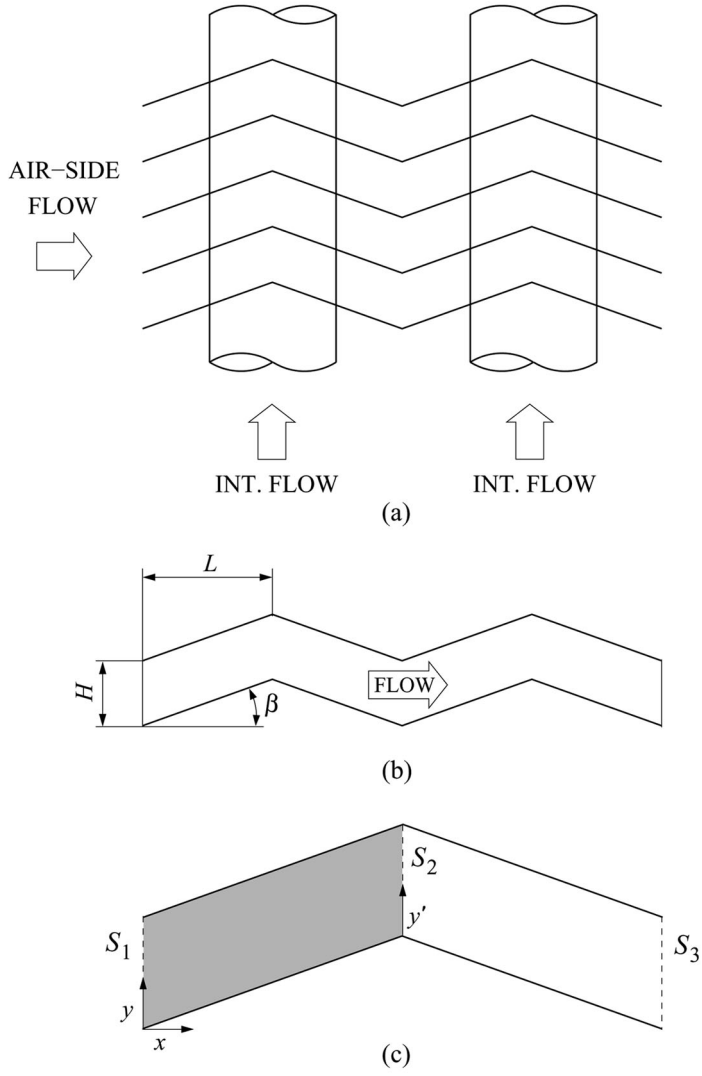

Figure 1.
Flow and convective heat and mass transfer in a typical tube-fin exchanger: (a) tube-fin geometry; (b) schematic two-dimensional representation of the geometry; (c) computational cell in the fully developed region

$$\frac{\partial v}{\partial \vartheta} + u\frac{\partial v}{\partial x} + v\frac{\partial v}{\partial y} = v\left(\frac{\partial^2 v}{\partial x^2} + \frac{\partial^2 v}{\partial y^2}\right) - \frac{1}{\rho}\frac{\partial p}{\partial y} \tag{2}$$

$$\frac{\partial u}{\partial x} + \frac{\partial v}{\partial y} = 0 \tag{3}$$

These equations, without any further modification, can be utilized for the analysis of the entrance region shown in Figure 1(b). In the fully developed flow region, the average pressure gradient is constant in the axial direction. Consequently, with reference to the situation shown in Figure 1(c), we can write

$$p(x,y) = -\alpha x + \tilde{p}(x,y) \tag{4}$$

as suggested by Patankar *et al.* (1977). In the above equation, α is a constant representing the overall pressure gradient in the main flow direction x, while $\tilde{p}$ is the periodic component of pressure.

On the basis of Equation (4), the momentum equations, governing the fully developed laminar flow of the humid air, can be modified as follows:

$$\frac{\partial u}{\partial \vartheta} + u\frac{\partial u}{\partial x} + v\frac{\partial u}{\partial y} = \nu\left(\frac{\partial^2 u}{\partial x^2} + \frac{\partial^2 u}{\partial y^2}\right) + \frac{1}{\rho}\left(\alpha - \frac{\partial \tilde{p}}{\partial x}\right) \tag{5}$$

$$\frac{\partial v}{\partial \vartheta} + u\frac{\partial v}{\partial x} + v\frac{\partial v}{\partial y} = \nu\left(\frac{\partial^2 v}{\partial x^2} + \frac{\partial^2 v}{\partial y^2}\right) - \frac{1}{\rho}\frac{\partial \tilde{p}}{\partial y} \tag{6}$$

Appropriate conditions must be imposed on wall, anti-periodic, inflow and outflow boundaries. On wall boundaries, we assume that the condensation induces a negligible transversal velocity. Furthermore, we neglect the thickness of the liquid film reflecting a "state of the art" in which there is no full agreement on the effects of a liquid film. In fact, the presence of a liquid film tends to increase the average axial velocity (reducing the heat convection resistance and increasing the friction factor). On the other hand, a liquid film also brings about an additional thermal resistance. Thus, as pointed out by Ramadhyani (1998), it is yet unclear whether liquid films enhance or diminish global convection coefficients, although it appears that they always increase friction factors. For the above reasons, the usual no-slip boundary condition

$$u = v = 0 \tag{7}$$

is adopted at solid walls. This way, the flow problem is fully decoupled from the heat and mass transfer problems. In particular, the flow field can be determined without dealing simultaneously with concentration and temperature distributions. However, it must be pointed out that, by decoupling the equations, we do not disregard the effects of mass transfer on energy exchanges. In fact latent heat fluxes, associated with mass concentration gradients at wall surfaces, can be taken into account in the same way as sensible heat fluxes related to temperature gradients, are accounted.

The anti-symmetric periodicity between the boundaries S_1 and S_2 yields the condition

$$\tilde{p}(L, H - y') = \tilde{p}(0, y) \tag{8}$$

where y' is the distance from the lower boundary measured in the y direction. As shown in Figure 1(c), H is the height, i.e. the fin pitch, and L is the projected length of one half-module. Similarly, on boundaries S_1 and S_2 we impose the conditions:

$$u(L, H - y') = u(0, y) \tag{9}$$

$$v(L, H - y') = -v(0, y) \tag{10}$$

In the analysis of the entrance region, we specify the inlet velocity components by assuming a uniform velocity field parallel to the x-axis

$$u = \bar{u}; \quad v = 0 \tag{11}$$

where $\bar{u}$ is the average value of the velocity component in the x-direction, evaluated as:

$$\bar{u} = \frac{1}{H} \int_0^H u \, \mathrm{d}y \tag{12}$$

On the contrary, in fully developed periodic flows, conditions (9) and (10) do not involve the specification of any inflow velocity. Therefore, the pressure gradient α must be adjusted iteratively, until the desired value of the virtual "inflow" velocity is reached as described by Nonino and Comini (1998).

Finally, in the analysis of the entrance region, we must specify also suitable outflow conditions at an artificial boundary by assuming, for example:

$$\frac{\partial u}{\partial \vartheta} + \bar{u} \frac{\partial u}{\partial x} = 0 \tag{13}$$

$$\frac{\partial v}{\partial \vartheta} + \bar{u} \frac{\partial v}{\partial x} = 0 \tag{14}$$

These advective conditions are written in terms of a constant phase speed $\bar{u}$, estimated as the average flow velocity in the main direction. By definition, they yield the "natural" zero normal derivative conditions in stationary problems.

The behaviour of the flow is determined by the Reynolds number

$$\mathrm{Re} = \frac{\bar{u} D_\mathrm{H}}{v} \tag{15}$$

where $D_\mathrm{H} = 2H$ is the hydraulic diameter. The pressure drop depends on the Reynolds number and, in this study, is expressed as

$$\Delta p = f \frac{mL}{D_\mathrm{H}} \frac{\rho \bar{u}^2}{2} \tag{16}$$

where f is the apparent friction factor, m is the number of half-modules considered and L is the projected length of a single half-module. From equation (16) it follows that, in the fully developed flow region, the apparent friction factor can be expressed as

$$f_\infty = \frac{\alpha D_H}{\rho \bar{u}^2/2} \tag{17}$$

since it is directly related to the pressure gradient α.

The temperature field

In the absence of volumetric heating, and neglecting the effects of viscous dissipation, the two-dimensional energy equation can be written as

$$\frac{\partial t}{\partial \vartheta} + u\frac{\partial t}{\partial x} + v\frac{\partial t}{\partial y} = a\left(\frac{\partial^2 t}{\partial x^2} + \frac{\partial^2 t}{\partial y^2}\right) \tag{18}$$

where a is the thermal diffusivity.

Appropriate conditions must be imposed on wall, periodic, inflow and outflow boundaries. On solid boundaries, we specify the wall temperature:

$$t = t_w \tag{19}$$

On the contrary, for anti-periodic boundaries S_1 and S_2 in the fully developed flow region, we cannot write any simple relationship of this kind. However, as illustrated by Nonino and Comini (1998), we can use the alternative relationship

$$\frac{t(L, H - y') - t_w}{t_b(L) - t_w} = \frac{t(0, y) - t_w}{t_b(0) - t_w} \tag{20}$$

which leads to the condition:

$$t(L, H - y') = \left[1 + \frac{t_b(L) - t_b(0)}{t_b(0) - t_w}\right] t(0, y) - \frac{t_b(L) - t_b(0)}{t_b(0) - t_w} t_w \tag{21}$$

In the above equations t_b is the bulk temperature, which can be conveniently defined as:

$$t_b = \frac{\int_0^H |u| t \, dy}{\int_0^H |u| \, dy} \tag{22}$$

Equation (21) contains two unknown quantities: the bulk temperature at inflow $t_b(0)$ and the difference between the bulk temperatures at outflow and inflow. Thus, in the solution process, we first impose the value of the bulk temperature

difference, and then iterate until convergence is reached for a value of $t_b(0)$ which verifies the periodicity condition.

In the analysis of the entrance region, we directly specify the inlet temperature by assuming

$$t = t_i = \text{const} \tag{23}$$

and we also specify a suitable outflow condition at an artificial boundary by assuming:

$$\frac{\partial t}{\partial \vartheta} + \bar{u}\frac{\partial t}{\partial x} = 0 \tag{24}$$

Once again, the advective condition (24) yields the "natural" zero normal derivative condition in stationary problems.

The Reynolds number and the Prandtl number $\mathrm{Pr} = \nu/a$ determine the behaviour of the temperature field. This behaviour is characterized by the overall, i.e. space averaged, Nusselt number, defined as

$$\mathrm{Nu} = \frac{\bar{h}D_H}{k} = \frac{2\bar{h}H}{k} \tag{25}$$

where the bar over the Nu symbol has been omitted. In the above equation, the average heat transfer coefficient is defined as suggested by Kelkar and Patankar (1987)

$$\bar{h} = \frac{q}{S\Delta t_{mt}} \tag{26}$$

on the basis of the absolute value q of the heat transfer rate, the projected area S (i.e. the area pertaining to the corresponding length of a plain channel), and the log-mean temperature difference:

$$\overline{\Delta t} = \Delta t_{ml} = \frac{[t_w - t_b(mL)] - [t_w - t_b(0)]}{\ln\{[t_w - t_b(mL)]/[t_w - t_b(0)]\}} \tag{27}$$

Obviously, m is equal to 1 when an anti-periodic domain is considered.

The heat transfer characteristics are often presented also in terms of the Colburn factor for heat transfer:

$$j = \frac{\mathrm{Nu}}{\mathrm{Re}\,\mathrm{Pr}^{1/3}} \tag{28}$$

However, it must be pointed out that in fully developed laminar flows in plain channels, the Nusselt number does not depend on the Reynolds and Prandtl numbers.

The mass concentration field

In the absence of fog formation, and for a constant value of the humid air density, the species conservation requirement can be written as

$$\frac{\partial \omega}{\partial \vartheta} + u\frac{\partial \omega}{\partial x} + v\frac{\partial \omega}{\partial y} = d\left(\frac{\partial^2 \omega}{\partial x^2} + \frac{\partial^2 \omega}{\partial y^2}\right) \tag{29}$$

where ω is the mass fraction of water vapour, and d is the binary diffusion coefficient for the mixture of dry air and water vapour.

Appropriate conditions must be imposed on wall and anti-periodic boundaries. Under dehumidifying conditions, the pressure of the water vapour at wall boundaries is equal to the saturation pressure at temperature t_w. Since the humid air behaves, approximately, as an ideal gas mixture, we have:

$$\omega = \frac{\rho_v(T_w)}{\rho} \cong \frac{p_v(T_w)/(R_v T_w)}{\rho} = \omega_w \tag{30}$$

On the anti-periodic boundaries S_1 and S_2, in the fully developed flow region, we cannot write any simple relationship of this kind. However, on the basis of equation (20) we have

$$\frac{\omega(L, H - y') - \omega_w}{\omega_b(L) - \omega_w} = \frac{\omega(0, y) - \omega_w}{\omega_b(0) - \omega_w} \tag{31}$$

which leads to the condition:

$$\omega(L, H - y') = \left[1 + \frac{\omega_b(L) - \omega_b(0)}{\omega_b(0) - \omega_w}\right]\omega(0, y) - \frac{\omega_b(L) - \omega_b(0)}{\omega_b(0) - \omega_w}\omega_w \tag{32}$$

In the above equation, ω_b is the bulk concentration, which can be conveniently defined as:

$$\omega_b = \frac{\int_0^H |u|\omega \, dy}{\int_0^H |u| \, dy} \tag{33}$$

Equation (32) contains two unknown quantities: the bulk concentration at inflow $\omega_b(0)$ and the difference between the bulk concentrations at outflow and inflow. Thus, in the solution process, we first impose the value of the bulk concentration difference, and then iterate until convergence is reached for a value of $\omega_b(0)$ which verifies the periodicity condition.

In the analysis of the entrance region, we directly specify the inlet concentration by assuming

$$\omega = \omega_i = \text{const} \tag{34}$$

and we also specify a suitable outflow condition at an artificial boundary by assuming:

$$\frac{\partial \omega}{\partial \vartheta} + \bar{u}\frac{\partial \omega}{\partial x} = 0 \tag{35}$$

Once again, the advective condition (35) yields the "natural" zero normal derivative condition in stationary problems.

The Reynolds number, defined by equation (15), and the Schmidt number $\mathrm{Sc} = \nu/d$ determine the behaviour of the concentration field. This behaviour is characterized by the overall, i.e. space averaged Sherwood number, defined as:

$$\mathrm{Sc} = \frac{\bar{h}_{\mathrm{m}} D_{\mathrm{H}}}{d} \tag{36}$$

where the bar has been omitted over the Sh symbol. In the above equation

$$\bar{h}_{\mathrm{m}} = \frac{\dot{m}}{\rho S \Delta \omega_{\mathrm{ml}}} \tag{37}$$

is the average mass transfer coefficient, $\dot{m}$ is the absolute value of the mass transfer rate, S is the projected area, and

$$\overline{\Delta\omega} = \Delta\omega_{\mathrm{ml}} = \frac{[\omega_{\mathrm{w}} - \omega_{\mathrm{b}}(mL)] - [\omega_{\mathrm{w}} - \omega_{\mathrm{b}}(0)]}{\ln\{[\omega_{\mathrm{w}} - \omega_{\mathrm{b}}(mL)]/[\omega_{\mathrm{w}} - \omega_{\mathrm{b}}(0)]\}} \tag{38}$$

is the log-mean concentration difference. Once again, m is equal to 1 when an anti-periodic domain is considered.

The mass transfer characteristics are often presented also in terms of a Colburn factor for mass transfer:

$$j_{\mathrm{m}} = \frac{\mathrm{Sh}}{\mathrm{Re}\,\mathrm{Sc}^{1/3}} \tag{39}$$

However, it must be pointed out that in fully developed laminar flows in plain channels, also the Sherwood number does not depend on the Reynolds and Schmidt numbers.

Numerical solution

In the solution procedure, the momentum, continuity and energy equations are dealt with by the equal-order, velocity–pressure algorithm for incompressible thermal flows described by Nonino and Comini (1997). As already pointed out, the velocity–pressure coupling is handled by a methodology that shares many features with the SIMPLE/SIMPLER algorithm, illustrated by Patankar (1980). At each new time step $(n+1)$ the pseudovelocity field $(\hat{u}, \hat{v}, \hat{w})$, obtained by neglecting the pressure gradients in the momentum equations, is computed

from the velocity field (u^n, v^n, w^n), which prevails at the end of the old time step (n). Then, by enforcing continuity on the pseudo-velocity field, a tentative pressure p^* is estimated and the momentum equations are solved for the tentative velocity field (u^*, v^*, w^*). Afterwards, continuity is enforced again to find pressure corrections p', which yield the final pressure $p^{n+1} = p^* + p'$. Pressure corrections are also used to find the velocity corrections (u', v', w') that $\ll$project $\gg$ (u^*, v^*, w^*) onto the divergence-free space ($u^{n+1} = u^* + u'$, $v^{n+1} = v^* + v'$, $w^{n+1} = w^* + w'$). Once the velocity field ($u^{n+1}, v^{n+1}, w^{n+1}$) has been found, the energy equation can be solved before moving to the next step.

As illustrated by Comini *et al.* (1994), the momentum and energy equations are particular versions of the general transport equation that can be written in the time-discretized form:

$$\gamma\frac{\phi^{n+1} - \phi^n}{\Delta\vartheta} + \gamma v^n\cdot[\tau_v\nabla\phi^{n+1} + (1 - \tau_v)\nabla\phi^n]$$
$$= \Gamma[\tau_\Gamma\nabla^2\phi^{n+1} + (1 - \tau_\Gamma)\nabla^2\phi^n] + \dot{s} \tag{40}$$

The properties γ and Γ, and the volumetric source rate $\dot{s}$ can be easily identified by inspection of the appropriate original equations. It should be noted, however, that the components of the pressure gradient are contained in the source terms of the momentum equations. The weighting factors τ_v and τ_Γ, both in the range from 0 to 1, allow the selection of different time-integration schemes. Finally, it must be pointed out that the pressure equation, the pressure correction equation, and the streamfunction equation are all particular versions of the Poisson equation, which can be obtained from equation (40) by assuming $\gamma = 0$ and $\tau_\Gamma = \Gamma = 1$.

The space discretization of the general transport equation is based on the Galerkin method. In fact, for each node i we obtain an integral form by weighting and integrating equation (40) over the computational domain. The application of Green's theorem to the diffusion terms at the right hand side of equation (40) yields the weak forms and allows the introduction of Neumann boundary conditions.

As usual, the unknown functions are approximated throughout the solution domain by means of the expansions

$$\phi = \sum N_j\phi_j \tag{41}$$

where ϕ_j stand for the nodal values, while N_j are interpolating functions. In the Bubnov-Galerkin method utilized here, N_j coincide with the weighting functions employed in the weak forms. Therefore no upwinding techniques are employed.

Substituting equation (41) into the appropriate weak forms, we arrive at systems of space discretized equations, which can be written as

$$\mathbf{H}\boldsymbol{\phi} = \mathbf{g} \tag{42}$$

$\boldsymbol{\varphi}$ is the vector of nodal values, $\mathbf{H}$ is the effective stiffness matrix, accounting for all homogeneous contributions, and $\mathbf{g}$ is the effective load vector, accounting for all nonhomogeneous contributions. Finally, the boundary conditions of the first kind at the walls are implemented in the usual way, e.g. see Comini *et al.* (1994). The anti-periodic boundary conditions are introduced as illustrated in detail by Nonino and Comini (1998). With reference to the corresponding points on the inflow (i) and outflow (o) boundaries we have

$$\phi_0 = B\phi_i + E \tag{43}$$

where the values of B and E can be easily inferred from the physical boundary conditions. Accordingly, the matrix $\mathbf{H}$ and the right hand side vector $\mathbf{g}$ in equation (42) are modified to take into account equation (43).

In the numerical simulations, the systems of linear equations, arising at each time step from the discretization process, were solved by means of iterative algorithms. The conjugate gradient squared (CGS) method, described by Howard *et al.* (1990), has been used to solve the discretized momentum and energy equati ons. The modified conjugate gradient method (MCG), illustrated by Gambolati (1988, p. 136) has been used to solve the symmetric systems obtained from the discretization of the Poisson equations. In both cases, preconditioned matrices have been obtained from an incomplete LU decomposition (ILU).

Results and discussion

As already pointed out, the aim of this work is to illustrate the physics of the convection process rather than the production of an exhaustive database of numerical results. Therefore, the examples concern several Reynolds number in the range $100 \leq \mathrm{Re} \leq 1,000$, but only the fin geometry shown in Figure 1 where we have: $L/H = 2.26$ and $\beta = 20°$. The humid air is characterized by the Prandtl and Schmidt number values: $\mathrm{Pr} = 0.718$ and $\mathrm{Sc} = 0.61$.

In the computations, we utilized the boundary conditions discussed in some detail in the previous sections. The program had already been validated by Nonino and Croce (1997), and Nonino and Comini (1998); Nonino *et al.* (1999). On the other hand, its accuracy has been assessed once again imposing periodicity conditions on a portion of a plain channel. In this way we obtained results for the fully developed situation that, as expected, are independent of the Reynolds and Prandtl number, and agree to the third digit with the analytical solutions: $\mathrm{Nu}_0 = 7.5407$ and $(f\,\mathrm{Re})_0 = 96.00$ reported by Shah and Bhatti (1987, p. 3.30). Before the final runs, grid independence was established on the basis of calculations in which the distance between grid points was

progressively reduced by 30 per cent from one simulation to another. When a further decrease led to a change in the average Nusselt numbers smaller that 1 per cent, the results were considered grid-independent. Similarly, time-step independence was established on the basis of preliminary calculations in which the dimensionless time step $\bar{u}\Delta\vartheta/L$ was progressively reduced by 30 per cent from one simulation to another. When a further decrease led to a change in the average Nusselt numbers smaller that 1 per cent, the results were considered independent also on the time step.

The mesh for the entrance region encompasses 12 modules but, to simplify the graphical representations, only one module is shown in Figure 2. As already pointed out, the mesh for the fully developed region encompasses a single half-module. For the present calculations we used structured grids of bilinear elements. A satisfactory independence of results from the grid was established on the basis of preliminary calculations in which the distance between grid points was progressively reduced by 30 per cent from one simulation to another. When a further decrease led to a change in the average Nusselt numbers smaller than 1 per cent, the results were considered to be grid-independent. For the final simulations, we used grids consisting of 33,426 nodes (with finer grid spacing near the walls) for the entrance region and 4,032 nodes (with uniform grid spacing) for the fully developed region. Time-step independence was established on the basis of preliminary calculations in which the dimensionless time step $\bar{u}\Delta\vartheta/L$, employed to advance in time, was progressively reduced by 30 per cent from one simulation to another. When a further decrease led to a change in the average Nusselt numbers smaller than 1 per cent, the results were considered to be independent on the time step. In the final simulations, the dimensionless values of the time step ($\bar{u}\Delta\vartheta/D_{\mathrm{H}}$) were equal to 0.05 for steady state flows and 0.025 for time-periodic flows.

In the interval of Reynolds number investigated, solutions were stationary up to a critical value of the Reynolds number $\mathrm{Re}_{\mathrm{cr}}$, and became time-periodic for $\mathrm{Re} > \mathrm{Re}_{\mathrm{cr}}$. In time-periodic situations, overall parameters were further averaged over a period (or a suitable time-interval), yielding single representative values. This way we obtained time averaged values

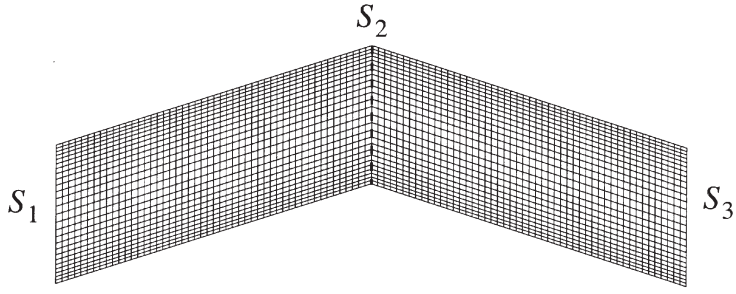

Figure 2.
Finite element discretization of a representative computational module

$$\langle \varphi \rangle = \frac{1}{\Theta} \int_{\vartheta}^{\vartheta+\Theta} \varphi(\vartheta) \mathrm{d}\vartheta \tag{44}$$

for $\varphi = f$, Nu, Sh, j or j_m. On the other hand, the symbol $\langle\ \rangle$ has been omitted in the following.

The entrance and the fully developed region

Wavy fins have a larger surface to volume ratio than plain fins of the same length and, at higher Reynolds numbers, leads to complex flow structures. These flow structures are reflected by the velocity, temperature, and concentration fields illustrated in Figures 3–5. Once again, to simplify

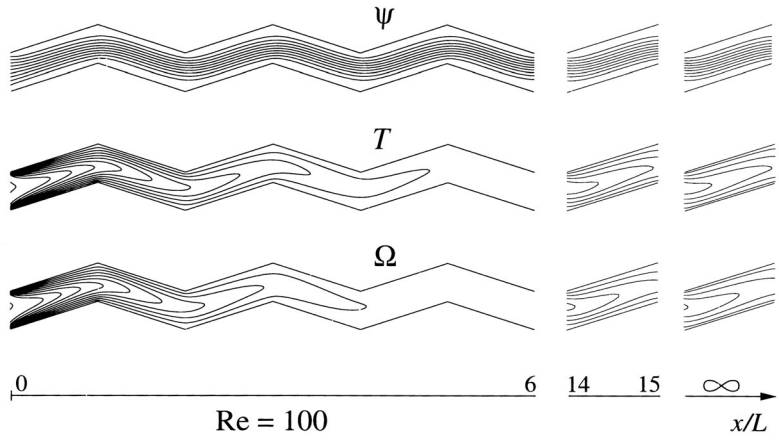

Figure 3.
Streamline contours (top), temperature contours (centre), and concentration contours (bottom) at Re = 100.

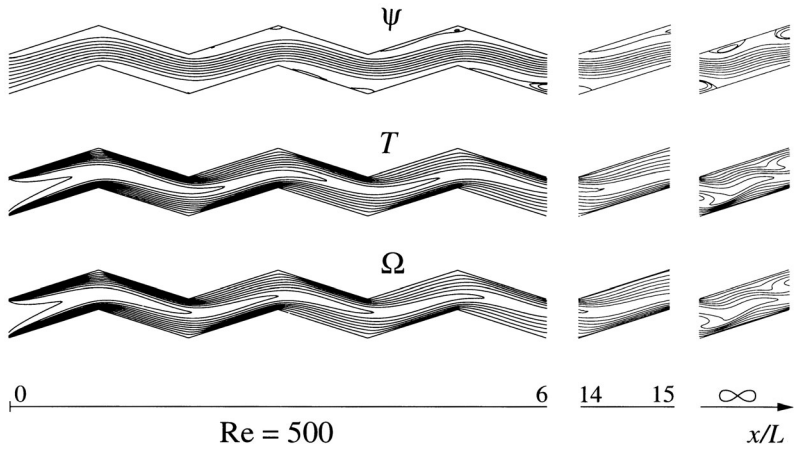

Figure 4.
Streamline contours (top), temperature contours (centre) and concentration contours (bottom) at Re = 500. Contours in the fully developed ($x/L = \infty$) region are instantaneous representations

graphical representations, we show the first three modules in the entrance region, a representative half-module at a reasonable distance from the entrance (the 15th half-module), and a half-module in the fully developed region (the mth half-module, for $m \rightarrow \infty$). The analysis was carried out for three Reynolds numbers: Re = 100, 500 and 1,000. These Reynolds numbers are in the range of greatest technical interest since they correspond, for example, to air velocities of 1 m/s, and reference lengths D_h varying from 1.5 to 15 mm.

At Re = 100, the flow is quite regular, as demonstrated by the streamline, temperature, and concentration contours shown in Figure 3. In the 15th half-module the streamline, temperature, and concentration fields do not differ in shape from the ones in the fully developed region. Heat and mass transfer enhancements, with respect to plain fins of equal length, are only due to the increase of the exchange surface per unit length, because of the regularity of the flow.

At Re = 500 the flow, temperature, and concentration fields become irregular, as demonstrated by the contours shown in Figure 4. In the 15th half-module the flow, temperature, and concentration fields are still steady, but they become unsteady in the fully developed region where vortex shedding occurs. As a consequence, in the fully developed region the contours are instantaneous representations of the flow conditions. The self-sustained flow oscillations, which take place in the fully developed region, are associated with transverse vortices that detach periodically and move downstream. This process transports fluid particles from the walls to the core and downstream, enhancing both heat and mass convection. The time behaviour of the transfer processes is shown in Figure 6, where we report the Nu vs. ϑ curve in the fully developed region and the corresponding power density spectrum. This spectrum is obtained from the FFT analysis referred to the peak-to-peak amplitude A_{Nu} of the Nusselt number oscillations. As we can see, the time behaviour is periodic with one dominant frequency. When expressed in terms of the Strouhal number

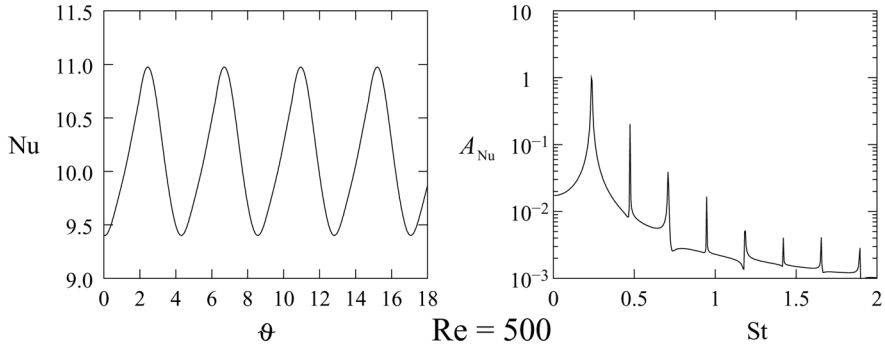

Figure 5.
Time behaviour of the space-averaged Nusselt number in the fully developed region (left), and corresponding power density spectrum (right) at Re = 500.

$$\mathrm{St} = \frac{D_h}{\bar{u}\Theta} \tag{45}$$

the dimensionless value of the dominant frequency is St ≅ 0.24.

At Re = 1,000 the irregularities in the flow, temperature, and concentration fields increase, as demonstrated by the contours shown in Figure 6. In both the 15th half-module, and in the half-module located in the fully developed region, flow, temperature, and concentration fields are unsteady, as can be inferred from their instantaneous representations. The time behaviour is shown in Figure 7 where we report, once again, the Nu vs. ϑ curve and the corresponding power density spectrum. As we can see, there is still one-dominant frequency, but the amplitude of the sub-harmonics has increased.

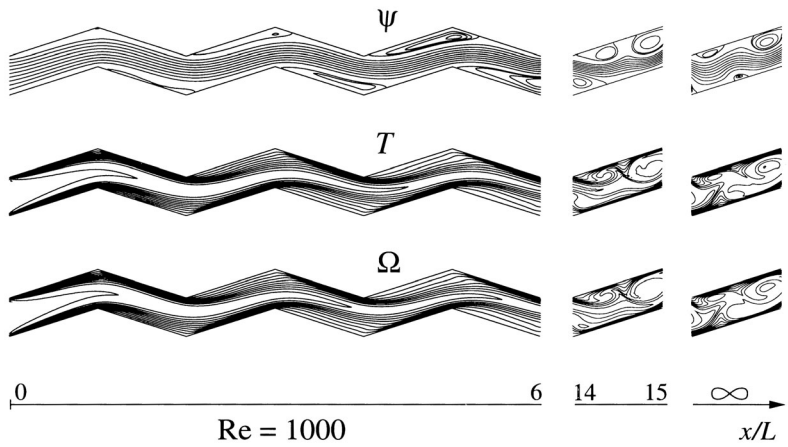

Figure 6.
Streamline contours (top), temperature contours (centre) and concentration contours (bottom) at Re = 1000. Contours in the 15th half module and in the fully developed region developed ($x/L = \infty$) region are instantaneous representations

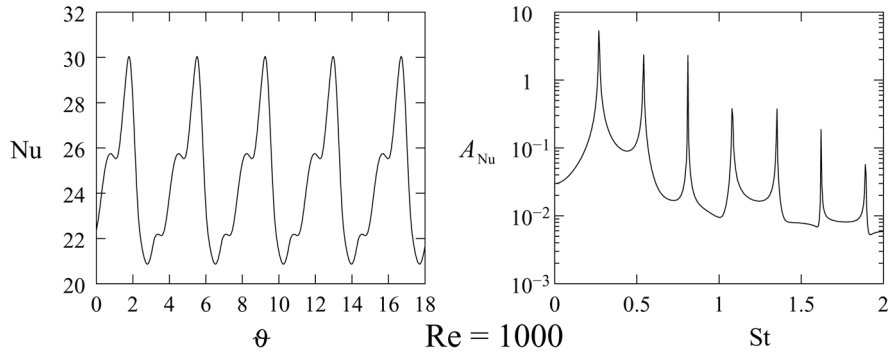

Figure 7.
Time behaviour of the space-averaged Nusselt number in the fully developed region (left), and corresponding power density spectrum (right) at Re = 1,000.

It must be pointed out that, at all Reynolds numbers, there is a striking resemblance between temperature and concentration solutions. In fact, under the assumptions made here, the only difference between heat and mass transfer models lies in the notation. Thus, by replacing the Nusselt number with the Sherwood number, and the Prandtl number with the Schmidt number, we may use convective heat transfer equations for convective mass transfer. This analogy is exploited in the heat transfer literature, as will be discussed in the next paragraph.

The irregularities in the flow patterns increase with the Reynolds number and influence the friction factor and the convection coefficients, both in the entrance and in the fully developed region. The behaviour of the friction factor is shown in Figure 8, where we plot the $f\,\mathrm{Re}$ parameters for wavy and plain fins as a function of the dimensionless variable:

$$x^{+} = \frac{x/D_{\mathrm{H}}}{\mathrm{Re}} \tag{46}$$

In plain fins, and in wavy fins for $\mathrm{Re} = 100$, the apparent friction factor decreases steadily from the entrance section to the fully developed region. On the contrary, for $\mathrm{Re} = 1,000$, we have a maximum in correspondence with the transition from steady to unsteady flow at $x^{+} \cong 0.015$. A similar behaviour can be expected for the $\mathrm{Re} = 500$ curve but, in this case, the transition occurs in the dashed zone, outside the regions investigated.

The behaviour of the convection coefficients can be illustrated by the behaviour of the average Nusselt number, as shown in Figure 9. The Nusselt numbers for wavy and plain fins are plotted as a function of the dimensionless variable:

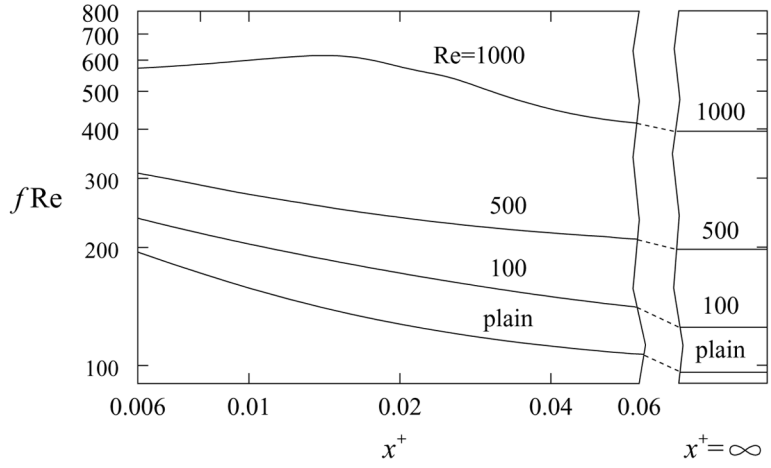

Figure 8.
Apparent friction factors in the entrance and in the fully developed region for wavy channels at $\mathrm{Re} = 100$, 500 and 1,000, and for plain channels at all Reynolds numbers

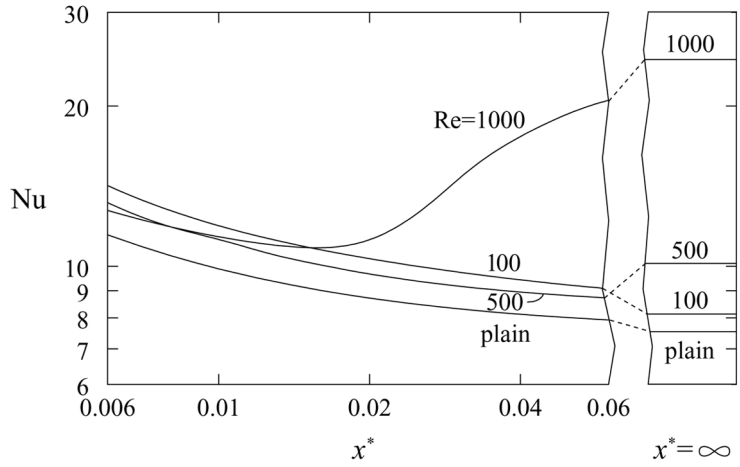

Figure 9.
Nusselt numbers in the entrance and in the fully developed region for wavy channels at Re = 100, 500 and 1000, and for plain channels at all Reynolds numbers

$$x^* = \frac{x/D_H}{\mathrm{Re}\,\mathrm{Pr}} \tag{47}$$

In plain fins, and in wavy fins for Re = 100, the average Nusselt number decreases steadily from the entrance section to the fully developed region. On the contrary, for Re = 1,000, we can see a minimum in correspondence with the transition from steady to unsteady flow at $x^* \cong 0.015$. A similar behaviour can be expected for the Re = 500 curve but, as already remarked, the transition occurs in the dashed zone, outside the regions investigated.

The heat and mass transfer analogy

As already pointed out, we may use convective heat transfer equations for convective mass transfer. In the literature, this analogy is applied to the fully developed flow region and is usually written in the form

$$\frac{j}{j_m} = \frac{(\mathrm{Nu}\,\mathrm{Pr}^{-1/3})/\mathrm{Re}}{(\mathrm{Sh}\,\mathrm{Sc}^{-1/3})/\mathrm{Re}} = \frac{\mathrm{Nu}}{\mathrm{Sh}}\left(\frac{\mathrm{Sc}}{\mathrm{Pr}}\right)^{1/3} = 1 \tag{48}$$

where j is the Colburn factor for heat transfer, j_m is the Colburn factor for mass transfer, and 1/3 is an experimentally determined exponent, e.g. see Incropera and De Witt (1996, p. 328). As can be inferred from Figure 10, our numerical results for the fully developed region tend to satisfy exactly the heat and mass convection analogy after the transition to oscillating flows has occurred at $\mathrm{Re} > \mathrm{Re}_{cr}$.

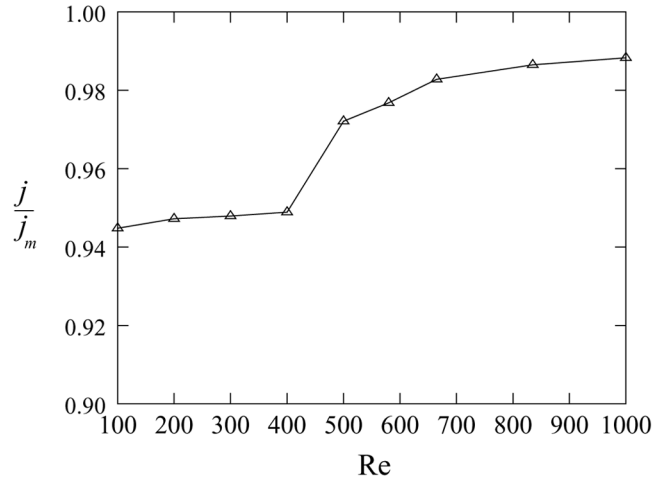

Figure 10.
Ratio j/j_m vs. the Reynolds number in the fully developed region

The influence of the Reynolds number

The influence of the Reynolds number on the momentum and heat transfer parameters is better investigated in the fully developed region. In Figure 11, we report the ratios f/f_0 and $\mathrm{Nu}/\mathrm{Nu}_0$, where f_0 and Nu_0 are the values for the corresponding plain fins. As can be seen, both the friction factor and the Nusselt number ratios increase with the Reynolds number. To evaluate the variations in performance, we might use the parameter

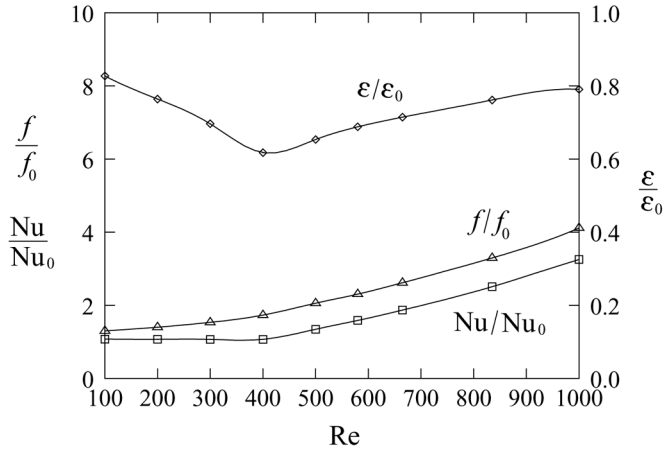

Figure 11.
Ratios f/f_0 and $\mathrm{Nu}/\mathrm{Nu}_0$, and goodness factor $\varepsilon/\varepsilon_0$ vs. the Reynolds number in the fully developed region

$$\varepsilon = \frac{j}{f} = \frac{\mathrm{Nu}}{\mathrm{Re}\,\mathrm{Pr}^{1/3}}\frac{1}{f} \tag{49}$$

which assumes the value

$$\varepsilon_0 = \frac{j_0}{f_0} = \frac{\mathrm{Nu}_0}{(f\,\mathrm{Re})_0\mathrm{Pr}^{1/3}} = 0.08772 \tag{50}$$

for fully developed laminar flow of air (Pr = 0.718) in plain channels. The ratio $\varepsilon/\varepsilon_0$, shown in Figure 11, can thus be used as a goodness factor since it represent the relative increase in heat transfer divided by the relative increase in pressure drop. As we can see, this goodness factor reaches a minimum just before the onset of the self-sustained oscillations.

Conclusions

Convective heat and mass transfer in laminar flows of humid air through plain and wavy fin channels has been investigated. A completely general approach has been followed, even though the finite element method has been used in the discretization process. Velocity, temperature, and concentration fields have been computed first. Quantitative results have then been obtained, for apparent friction factors, Nusselt numbers, Colburn factors, and goodness factors. This way, it has been found that heat and mass transfer analogy holds good for the fully developed region after the transition to oscillatory flows has occurred at $\mathrm{Re} > \mathrm{Re}_{cr}$, and that the goodness factor reaches a minimum just before the onset of the self-sustained oscillations.

References

Ali, M.M. and Ramadhyani, S. (1992), "Experiments on convective heat transfer in corrigated channels", *Exp. Heat Transfer*, Vol. 5, pp. 175-93.

Comini, G., Del Giudice, S. and Nonino, C. (1994), *Finite Element Analysis in Heat Transfer: Basic Formulation and Linear Problems*, Taylor and Francis, Washington, DC.

Gambolati, G. (1988), *Elements of Numerical Analysis*, (in Italian) Libreria Cortina, Padova, Ialy.

Howard, D., Connolley, W.M. and Rollett, J.S. (1990), "Unsymmetric conjugate gradient methods and sparse direct methods in finite element flow simulations", *Int. J. Numer. Meth. Fluids*, Vol. 10, pp. 925-45.

Hu, X., Zhang, L. and Jacobi, A.M. (1994), "Suface irregularity effects of droplets and retained condensate on local heat transfer to finned tubes in cross-flow", *ASHRAE Trans.*, Vol. 118–1, pp. 375-81.

Incropera, F.P. and DeWitt, D.P. (1996), *Fundamentals of Heat and Mass Transfer*, Wiley, New York.

Kelkar, K.M. and Patankar, S.V. (1987), "Numerical prediction of periodically fully developed flow and heat transfer in a parallel plate channel with staggered fins", *J. Heat Transfer*, Vol. 109, pp. 25-30.

Nonino, C. and Comini, G. (1997), "An equal order pressure-velocity algorithm for incompressible thermal flows – Part 1: formulation", *Numer. Heat Transfer, Part B*, Vol. 32, pp. 1-15.

Nonino, C. and Comini, G. (1998), "Finite-element analysis of convection problems in spatially periodic domains", *Numer. Heat Transfer, Part B*, Vol. 34, pp. 361-78.

Nonino, C. and Comini, G. (2000), "Heat transfer in channels with transverse and angled ribs", in, *3rd European Thermal Sciences Conference*, Hahne, E.W.P., Heidemann, W., Spindler, K., (Eds) Edizioni ETS, Pisa Volume Vol. 1 pp. 319-24.

Nonino, C. and Croce, G. (1997), "An equal order pressure-velocity algorithm for incompressible thermal flows – Part 2: validation", *Numer. Heat Transfer, Part B*, Vol. 32, pp. 17-35.

Nonino, C., Comini, G. and Croce, G. (1999), "Three-dimensional flows over backward facing steps", *Int. J. Nume. Meth. Heat Fluid Flow*, Vol. 9, pp. 224-39.

Patankar, S.V. (1980), *Numerical Heat Transfer and Fluid Flow*, Hemisphere, Washington, D.C..

Patankar, S.V., Liu, C.H. and Sparrow, E.M. (1977), "Fully developed flow and heat transfer in ducts having streamwise-periodic variations of cross-sectional area", *Trans. ASME, J. Heat Transfer*, Vol. 99, pp. 180-6.

Ramadhyani, S. (1998), "Calculation of air-side heat transfer in compact heat exchangers under condensing conditions", in, *Computer Simulations in Compact Heat Exchangers*, Chapter 6. Sundén, B., Fahgri, M., (Eds) Computational Mechanics Publications, Southampton, U.K. pp. 151-68.

Shah, R.K. and Bhatti, M.S. (1987), "Laminar convective heat transfer in ducts", in, *Handbook of Single-Phase Convective Heat Transfer*, Chapter 3. Kakac, S., Shah, R.S., Aung, W., (Eds) Wiley, New York.

Webb, R.L. *Principles of Enhanced Heat Transfer*, Wiley, New York.